

# Diffusional Kurtosis Imaging: The Quantification of Non-Gaussian Water Diffusion by Means of Magnetic Resonance Imaging

Jens H. Jensen,<sup>1\*</sup> Joseph A. Helpert,<sup>1</sup> Anita Ramani,<sup>1</sup> Hanzhang Lu,<sup>1</sup> and Kyle Kaczynski<sup>2</sup>

**A magnetic resonance imaging method is presented for quantifying the degree to which water diffusion in biologic tissues is non-Gaussian. Since tissue structure is responsible for the deviation of water diffusion from the Gaussian behavior typically observed in homogeneous solutions, this method provides a specific measure of tissue structure, such as cellular compartments and membranes. The method is an extension of conventional diffusion-weighted imaging that requires the use of somewhat higher  $b$  values and a modified image postprocessing procedure. In addition to the diffusion coefficient, the method provides an estimate for the excess kurtosis of the diffusion displacement probability distribution, which is a dimensionless metric of the departure from a Gaussian form. From the study of six healthy adult subjects, the excess diffusional kurtosis is found to be significantly higher in white matter than in gray matter, reflecting the structural differences between these two types of cerebral tissues. Diffusional kurtosis imaging is related to  $q$ -space imaging methods, but is less demanding in terms of imaging time, hardware requirements, and postprocessing effort. It may be useful for assessing tissue structure abnormalities associated with a variety of neuropathologies. *Magn Reson Med* 53:1432–1440, 2005. © 2005 Wiley-Liss, Inc.**

**Key words:** MRI; diffusion; kurtosis; brain; non-Gaussian; neuropathology

The diffusion of water through a biologic tissue can be regarded as a random process. Hence, the chance of a particular water molecule diffusing from one location to another in a given period of time is governed by a probability distribution. In the simplest models, this distribution has a Gaussian form with its width (i.e., standard deviation) proportional to the diffusion coefficient. However, for time intervals on the order of tens of milliseconds, the complex structure of most tissues, consisting of various types of cells and their membranes, can cause the diffusion displacement probability distribution to deviate substantially from a Gaussian form (1). This deviation from Gaussian behavior can be quantified using a convenient dimensionless metric called the excess kurtosis. Since the deviation from Gaussian behavior is governed by

the complexity of the tissue within which the water is diffusing, this excess diffusional kurtosis can be regarded as a measure of a tissue's degree of structure.

In this article, we describe a method, which has previously been presented in an abbreviated form (2), for estimating the excess kurtosis of water diffusion in vivo by means of pulsed-field-gradient MRI. We term this method diffusional kurtosis imaging (DKI). The method is based on the same type of pulse sequences employed for conventional diffusion-weighted imaging (DWI), but the required  $b$  values are somewhat larger than those usually used to measure diffusion coefficients. In the brain,  $b$  values of about 2000 s/mm<sup>2</sup> are sufficient, which can now be readily obtained on modern clinical MRI systems. Thus, DKI provides a practical clinical technique for quantifying non-Gaussian water diffusion and thereby for probing the microscopic structure of biologic tissues.

DKI has a close relationship to  $q$ -space imaging techniques (3), and  $q$ -space imaging methods have indeed recently been employed to estimate diffusional kurtosis (4,5). The principal difference between  $q$ -space imaging and the approach presented here is that  $q$ -space imaging seeks to estimate the full diffusion displacement probability distribution rather than just the kurtosis. As a consequence,  $q$ -space imaging is more demanding in terms of imaging time and gradient strengths. A key idea of the work presented here is that the excess diffusional kurtosis may be approximately determined from just the first three terms of an expansion of the logarithm of the NMR signal intensity in powers of  $b$ . It is for this reason that measuring the diffusional kurtosis requires only modest increases in  $b$  values beyond those typically employed for DWI.

In addition to presenting the underlying theory of DKI, we also show parametric maps of excess diffusional kurtosis in the human brain and in a phantom. In particular, we find sharp differences between the diffusional kurtosis in white and gray matter, confirming the preliminary results reported by Jensen and Helpert (2). We believe that DKI is potentially of value for the assessment of neurologic diseases, such as multiple sclerosis and epilepsy, with associated white matter abnormalities. Additionally, DKI may be useful for investigating abnormalities in tissues with isotropic structure, such as gray matter, where techniques like diffusion tensor imaging (DTI) are less applicable.

## THEORY

### Definition of Diffusional Kurtosis

Consider water molecules diffusing within a selected region of interest. If the initial position of a water molecule

<sup>1</sup>Department of Radiology, Center for Biomedical Imaging, New York University School of Medicine, New York, New York, USA.

<sup>2</sup>Siemens Medical Solutions USA, Parsippany, New Jersey, USA.

Grant sponsor: Institute for the Study of Aging; Grant sponsor: Werner Dannheisser Testamentary Trust.

\*Correspondence to: Jens H. Jensen, Department of Radiology, New York University School of Medicine, KIP-600-A, 650 First Avenue, New York, NY 10016-3240, USA. Email: jens.jensen@med.nyu.edu

Received 2 July 2004; revised 10 January 2005; accepted 20 January 2005.

DOI 10.1002/mrm.20508

Published online in Wiley InterScience (www.interscience.wiley.com).

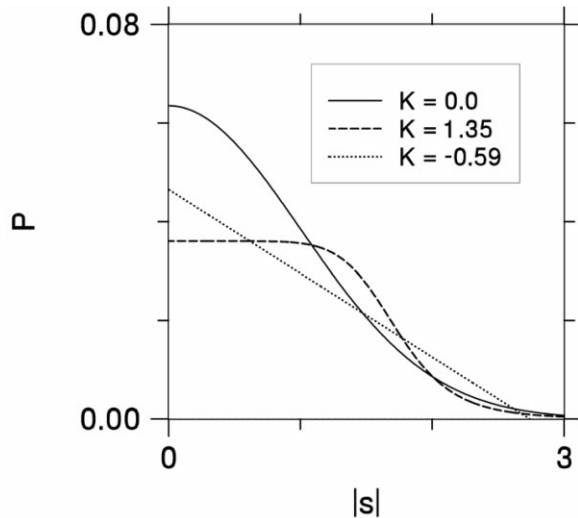


FIG. 1. Three isotropic diffusion displacement probability distributions. The corresponding diffusion coefficients are identical, but the values for diffusional kurtosis as calculated from Eq. [2] are different. The solid curve with  $K = 0$  is the Gaussian form obtained by setting  $Dt = 1/2$  in Eq. [3].

is  $\mathbf{r}_a$  and the final position is  $\mathbf{r}_b$ , then the net displacement is  $\mathbf{s} = \mathbf{r}_b - \mathbf{r}_a$ . Let  $P(\mathbf{s}, t)$  be the probability that a water molecule diffuses a given net displacement in a time  $t$ . The average value of an arbitrary function  $F(\mathbf{s})$  is

$$\langle F(\mathbf{s}) \rangle = \int d^3s P(\mathbf{s}, t) F(\mathbf{s}). \quad [1]$$

Now suppose we are interested in diffusion in a particular direction specified by a unit vector  $\mathbf{n}$ . Then the excess diffusional kurtosis in this direction is

$$K(t) = \frac{\langle (\mathbf{n} \cdot \mathbf{s})^4 \rangle}{\langle (\mathbf{n} \cdot \mathbf{s})^2 \rangle^2} - 3. \quad [2]$$

Equation [2] represents a straightforward application of the general definition of the excess kurtosis to diffusion (6,7). The term “excess kurtosis” is often shortened to “kurtosis,” although kurtosis is also sometimes used to mean just the first term on the right-hand-side of Eq. [2]. Here we use “excess diffusional kurtosis” and “diffusional kurtosis” interchangeably to refer to  $K(t)$ .

For isotropic Gaussian diffusion,

$$P(\mathbf{s}, t) = (4\pi Dt)^{-3/2} \exp(-\mathbf{s} \cdot \mathbf{s} / 4Dt), \quad [3]$$

where  $D$  is the diffusion coefficient. In this case, one may readily show that  $K(t)$  vanishes. If  $P$  is more sharply peaked than a Gaussian,  $K$  is negative, and if  $P$  is less sharply peaked than a Gaussian,  $K$  is positive (6,7). Thus  $K$  provides a dimensionless metric of the degree to which the diffusion displacement probability distribution is non-Gaussian. Figure 1 shows examples of three isotropic displacement probability distributions with identical diffu-

sion coefficients, but different values of  $K$ . The diffusion coefficient in a direction  $\mathbf{n}$  is, in general, defined by

$$D(t) = \frac{1}{2t} \langle (\mathbf{n} \cdot \mathbf{s})^2 \rangle. \quad [4]$$

### Diffusional Kurtosis and the NMR Signal

Consider a standard pulsed-field-gradient NMR sequence with a gradient strength  $g$ , a pulse duration  $\delta$ , and a time interval  $\Delta$  between the centers of the diffusion sensitizing gradient pulses (8). The central result of this paper is that this type of sequence can be used to approximately measure the diffusional kurtosis. The key relationship is

$$\ln [S(b)] = \ln [S(0)] - bD_{\text{app}} + \frac{1}{6} b^2 D_{\text{app}}^2 K_{\text{app}} + O(b^3), \quad [5]$$

where  $S(b)$  is the signal intensity at the echo time,  $D_{\text{app}}$  is the apparent diffusion coefficient, and  $K_{\text{app}}$  is the apparent diffusional kurtosis (2). The parameter  $b$  is given by the usual expression  $b = (\gamma\delta g)^2 (\Delta - \delta/3)$ , where  $\gamma$  is the proton gyromagnetic ratio. In carrying out the expansion of Eq. [5], it is assumed that  $b$  is changed by varying the gradient strength  $g$  with the timing parameters  $\delta$  and  $\Delta$  being kept fixed. Just as  $D_{\text{app}}$  is an estimate for the diffusion coefficient in the direction parallel to the orientation of diffusion sensitizing gradients,  $K_{\text{app}}$  is an estimate for the diffusional kurtosis in this same direction.

More precisely,

$$K(\Delta) = \lim_{\delta \rightarrow 0} K_{\text{app}}(\Delta, \delta), \quad [6]$$

so that the apparent diffusional kurtosis approaches the true diffusional kurtosis in the limit of short gradient pulse durations, which is analogous to the relationship between  $D_{\text{app}}$  and the true water diffusion coefficient  $D$ . The validity of Eq. [6] requires that there is no net flow, which implies  $\langle \mathbf{s} \rangle = 0$  for all times  $t$ , and that the effects of inhomogeneous  $T_2$  relaxation are negligible. The derivation of Eq. [6] is outlined in the Appendix.

The expansion of Eq. [5] is essentially a Taylor expansion of  $\ln[S(b)]$  in powers of  $b$ . Similar expansions have been previously considered by Yablonskiy et al. (9) and by Liu et al. (10). However, neither of these works makes the connection to the diffusional kurtosis, which was originally observed by Jensen and Helpert (2).

### Special Cases

As an example, consider a region of interest consisting of  $N$  noninteracting compartments, each containing a fraction  $p_i$  ( $i = 1, 2, \dots, N$ ) of the water molecules. Assume that the diffusion is Gaussian in each compartment with a diffusion coefficient  $D_i$ . Then the diffusional kurtosis is simply

$$K(t) = 3 \frac{\text{var}(D)}{\bar{D}^2}, \quad [7]$$

with

$$\bar{D} = \sum_{i=1}^N p_i D_i, \quad \text{var}(D) = \sum_{i=1}^N p_i (D_i - \bar{D})^2. \quad [8]$$

So in this case, the diffusional kurtosis reflects diffusional heterogeneity. It may also be noted that for this particular model  $K_{\text{app}}(\Delta, \delta) = K(\Delta)$  so that the expansion of Eq. [5] will yield the exact diffusional kurtosis for any duration  $\delta$  of the gradient pulses.

In biologic tissues, the diffusional kurtosis may be affected by the exchange of water between compartments (e.g., the extracellular and intracellular spaces). This can be illustrated by using the two-compartment exchange model studied by Karger (1) and by Lee and Springer (11). For this model, one may derive the expression

$$K(t) = 6 \frac{\text{var}(D)}{\bar{D}^2} \cdot \frac{1}{\alpha} \left[ 1 - \frac{1}{\alpha} (1 - e^{-\alpha}) \right], \quad [9]$$

where  $\alpha = t/(\tau_a p_b) = t/(\tau_b p_a)$ . Here  $\tau_a$  and  $\tau_b$  are the water residence times for the two compartments, and  $p_a$  and  $p_b$  ( $= 1 - p_a$ ) are the corresponding water fractions. The time  $\tau_m = \tau_a p_b = \tau_b p_a$  is the water mixing time for the system. The diffusional kurtosis of Eq. [9] approaches that of Eq. [7] for  $t \ll \tau_m$  and decreases as  $1/t$  for  $t \gg \tau_m$ . Thus water exchange decreases the diffusional kurtosis for long times.

In both of the above examples, the diffusional kurtosis is nonnegative. However, negative values are not strictly excluded. For instance, suppose the region of interest consists of water confined to spherical pores all with the same radius. For long times, the water molecules will be uniformly distributed within each of the pores. In this limit, one may show that the diffusional kurtosis approaches  $-3/7$ , implying that the diffusion displacement probability distribution is more sharply peaked than a Gaussian distribution. If the region of interest consists of spherical pores of two different radii,  $R_a$  and  $R_b$ , and water fractions,  $p_a$  and  $p_b$ , then for long times the diffusional kurtosis is given by

$$\lim_{t \rightarrow \infty} K(t) = \frac{18}{7} \cdot \frac{p_a R_a^4 + p_b R_b^4}{(p_a R_a^2 + p_b R_b^2)^2} - 3, \quad [10]$$

If  $0.67188 < R_b/R_a < 1.48837$ , the diffusional kurtosis of Eq. [10] is negative for all values of the water fractions. However, outside this range, the water fractions can be chosen to make  $K$  positive. So the heterogeneity of having two substantially different pore sizes can dominate the narrowing of the probability distribution caused by the restricted diffusion. The maximum kurtosis occurs when  $p_a = R_b^2/(R_b^2 + R_a^2)$ .

These examples suggest that the diffusional kurtosis tends to increase with diffusional heterogeneity and can be altered by water exchange or by diffusion barriers. It should also be noted that the kurtosis may have a complex temporal variation and can even change from being positive to negative with increasing time. The derivations of Eqs. [7], [9], and [10] are discussed in the Appendix.

## Diffusional Kurtosis Tensor

In general, the measured diffusional kurtosis may depend on the direction of the diffusion sensitizing gradients. This dependence on direction can be described by a tensor with 15 independent components, just as the directional dependence of the diffusion coefficient can be described by a tensor with 6 independent components (12). In order to determine the full diffusional kurtosis tensor, the diffusional kurtosis must therefore be measured in at least 15 different directions.

We define the diffusional kurtosis tensor to be

$$W_{ijkl}(t) = 9 \frac{\langle s_i s_j s_k s_l \rangle - \langle s_i s_j \rangle \langle s_k s_l \rangle - \langle s_i s_k \rangle \langle s_j s_l \rangle - \langle s_i s_l \rangle \langle s_j s_k \rangle}{\langle \mathbf{s} \cdot \mathbf{s} \rangle^2}, \quad [11]$$

with  $s_j$  indicating a component of the displacement vector  $\mathbf{s}$ . The diffusional kurtosis tensor has a rank of 4 and 81 components. Because it is fully symmetric with respect to an interchange of indices, only 15 components are independent. From Eqs. [2] and [11], one sees that

$$K(t) = \frac{\left[ \frac{1}{3} \sum_{i=1}^3 D_{ii}(t) \right]^2}{\left[ \sum_{i=1}^3 \sum_{j=1}^3 n_i n_j D_{ij}(t) \right]^2} \cdot \sum_{i=1}^3 \sum_{j=1}^3 \sum_{k=1}^3 \sum_{l=1}^3 n_i n_j n_k n_l W_{ijkl}(t), \quad [12]$$

where  $n_i$  is a component of the direction vector  $\mathbf{n}$  and

$$D_{ij}(t) = \frac{1}{2t} \langle s_i s_j \rangle, \quad [13]$$

is the diffusion tensor. Hence if  $D_{ij}$  and  $W_{ijkl}$  are known, then the kurtosis in any direction can be determined. For isotropic diffusion, Eqs. [11] and [12] imply

$$W_{ijkl}(t) = \frac{1}{3} (\delta_{ij} \delta_{kl} + \delta_{ik} \delta_{jl} + \delta_{il} \delta_{jk}) K(t). \quad [14]$$

In analogy to Eq. [5], the apparent diffusion and diffusional kurtosis tensors are derived from the expansion

$$\begin{aligned} \ln[S(b)] &= \ln[S(0)] - b \sum_{i=1}^3 \sum_{j=1}^3 n_i n_j D_{ij}^{\text{app}} \\ &+ \frac{1}{6} b^2 \left( \frac{1}{3} \sum_{i=1}^3 D_{ii}^{\text{app}} \right)^2 \sum_{i=1}^3 \sum_{j=1}^3 \sum_{k=1}^3 \sum_{l=1}^3 n_i n_j n_k n_l W_{ijkl}^{\text{app}} + O(b^3). \quad [15] \end{aligned}$$

In the limit of short durations for the gradient pulses, the apparent diffusion and diffusional kurtosis tensors approach their ideal values given by Eqs. [11] and [13]. The expansion of Eq [15], is similar to one discussed by Liu et al. (10).

Table 1  
MRI Estimates for the Mean Diffusional Kurtosis and Diffusion Coefficient Obtained from Six Subjects

Region	Direction	Diffusional kurtosis	Diffusion coefficient ( $\mu\text{m}^2/\text{ms}$ )
Cortical gray matter	Phase	$0.86 \pm 0.27$	$0.74 \pm 0.38$
Cortical gray matter	Read	$0.80 \pm 0.09$	$0.82 \pm 0.12$
Cortical gray matter	Slice	$0.79 \pm 0.07$	$0.76 \pm 0.08$
Frontal white matter	Phase	$1.33 \pm 0.22$	$0.96 \pm 0.16$
Frontal white matter	Read	$1.31 \pm 0.17$	$0.91 \pm 0.10$
Frontal white matter	Slice	$1.60 \pm 0.25$	$0.78 \pm 0.06$

Note. The uncertainties indicate standard deviations.

## METHODS

### Human Studies

Our human studies were performed using a Siemens 3.0-T Allegra MRI scanner and were approved by the institutional review board. Dual spin echo diffusion-weighted 2D EPI images were acquired with  $b$  values of 0, 500, 1000, 1500, 2000, and 2500  $\text{s}/\text{mm}^2$  in six healthy adult volunteers, who all gave informed consent. The images were oriented axially with a slight tilt. For all the subjects, three sets of images were obtained, each with a different direction (phase, read, and slice) for the diffusion sensitizing gradients. The phase encoding direction was from anterior to posterior. The acquisition matrix was  $128 \times 128$ , the voxels were isotropic with a volume of  $8 \text{ mm}^3$ , 3/4 partial Fourier encoding was employed, and each image was obtained by averaging the data from 12 excitations. The timing parameters were  $\text{TE} = 106 \text{ ms}$ ,  $\Delta = 36.1 \text{ ms}$ , and  $\delta = 34.5 \text{ ms}$ . The diffusion time interval  $\Delta$  is here not defined precisely in the same manner as for a standard Stejskal–Tanner sequence, since a dual spin echo sequence was employed to reduce eddy currents (13). Rather,  $\Delta$  has been calculated so that the usual expression  $b = (\gamma\delta g)^2(\Delta - \delta/3)$  remains valid.

Parametric maps of  $D_{\text{app}}$  and  $K_{\text{app}}$  were created by fitting the image signal intensities on a voxel-by-voxel basis to the formula

$$S_{\text{exp}} = \left\{ \eta^2 + \left[ S_0 \exp \left( -bD_{\text{app}} + \frac{1}{6}b^2D_{\text{app}}^2K_{\text{app}} \right) \right]^2 \right\}^{1/2}, \quad [16]$$

where  $S_{\text{exp}}$  is the experimental signal intensity and  $\eta$  is the background noise. Equation [16] was fit to the data using the Levenberg–Marquardt method (7) with  $S_0$ ,  $D_{\text{app}}$ , and  $K_{\text{app}}$  as free parameters. The noise parameter  $\eta$  was estimated from the mean signal intensity in air. This procedure should give reliable estimates for  $K_{\text{app}}$  provided an appropriate range of  $b$  values is used. The  $b$  values should be large enough so that the effect of the  $O(b^2)$  term in the exponential is large compared to that of the noise, but the  $b$  values should be small enough so that the excluded  $O(b^3)$  term (cf. Eq. [5]) is negligible.

Region of interest analyses were carried out in both cortical gray matter and frontal white matter to obtain quantitative estimates for typical values for the diffusion coefficient and the diffusional kurtosis. For the intersubject comparisons used to construct Table 1, regions of interest were chosen by eye, with the assistance of a neuroradiologist, containing 10 voxels for gray matter and 12

voxels for white matter. White matter regions of interest were circular, but gray matter regions of interest were irregular due to the thinness of this structure. The signal intensities within each region of interest were averaged prior to fitting with Eq. [16].

### Phantom Study

A phantom was constructed consisting of six 60-mL plastic bottles submerged in a water bath. One bottle contained pureed asparagus to simulate an isotropic tissue with a nonzero kurtosis. The remaining five bottles contained sucrose solutions with sucrose concentrations of 5, 10, 15, 20, and 25%. Sucrose lowers the water diffusion coefficient (14), but is not expected to affect the diffusional kurtosis. The phantom was imaged on a Siemens 3.0-T Trio MRI scanner using the same type of sequence and  $b$  values as for the human studies. The image parameters were  $\text{TE} = 108 \text{ ms}$  and slice thickness = 5 mm; the acquisition matrix was  $128 \times 128$ , and the field of view was  $256 \times 256 \text{ mm}$ . Images were postprocessed in the same manner as for the human studies.

## RESULTS

### Human Studies

Figure 2 shows the signal intensity as a function of  $b$  in gray and white matter regions of interest for one subject. The region of interest for cortical gray matter contained 17 voxels, while the region of interest for frontal white matter contained 19 voxels (these regions of interest were optimized for this particular subject and are somewhat larger than those used for the construction of Table 1). A clear departure from monoexponential behavior is apparent in both gray and white matter, indicating a substantial deviation from Gaussian diffusion. The lines are fits to Eq. [16], showing that the data are well described by the theoretical form. A marked degree of directional anisotropy is apparent in white matter.

The robustness of our estimates for the diffusional kurtosis is illustrated by the uncertainties indicated in Fig. 2. For the results in this figure the fractional errors range from 7 to 17%. This level of precision is typical for our method. However, the precision of diffusional kurtosis estimates decreases rapidly if the maximum  $b$  values are reduced substantially below 2000  $\text{s}/\text{mm}^2$ .

Parametric maps of the apparent diffusional kurtosis and the apparent diffusion coefficient for the three orthogonal directions are given in Fig. 3 for one subject. The last

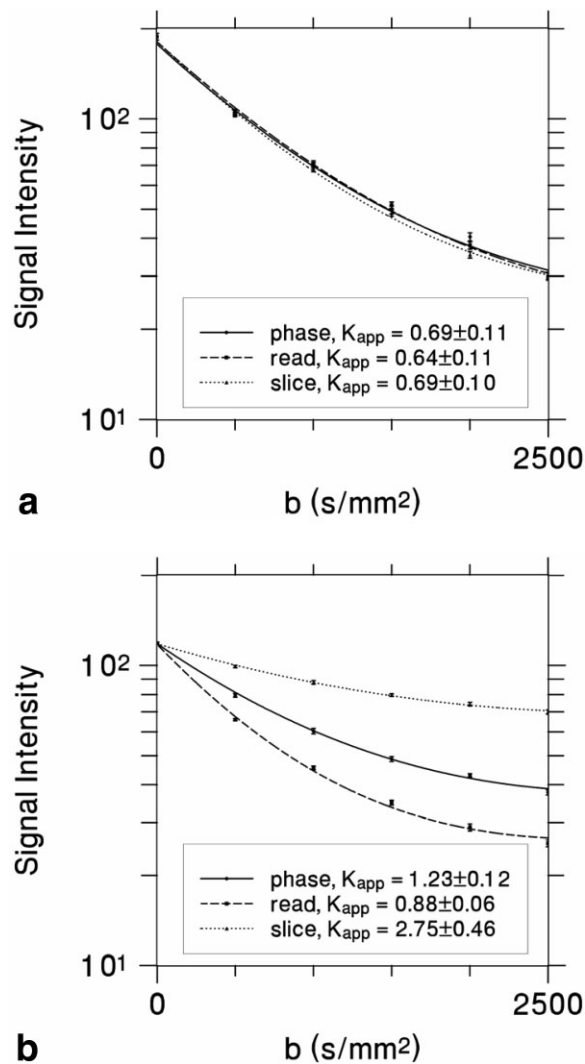


FIG. 2. Signal intensity versus  $b$  in three orthogonal directions for (a) cortical gray matter and (b) frontal white matter obtained from two regions of interest in one subject. The lines are fits using Eq. [16]. The apparent diffusional kurtosis is nearly isotropic for gray matter, but depends strongly on direction for white matter. The uncertainties in  $K_{app}$  are standard error estimates.

column shows the average over all three directions. The maps have been slightly smoothed to reduce the effect of noise and have been windowed so that voxels with negative values appear black. In a few voxels, the diffusional kurtosis did converge to negative values, but these may be artifacts of noise or other confounding effects. As previously discussed, negative values for the diffusional kurtosis are allowed theoretically, but our results suggest a predominance of positive values. The hyperintense circular feature apparent on the upper left side of the diffusional kurtosis map (subject's right brain side) in the slice direction is similar to features observed in other subjects. The asymmetry of the image may be due to the slice orientation or intrinsic asymmetry of the brain. For all the subjects of this study, the raw diffusion-weighted images were evaluated by a neuroradiologist and judged to be normal.

Figure 4 shows a scatter plot of the average  $K_{app}$  versus the average  $D_{app}$  obtained from the all the positive-value voxels of the images in Fig. 3. The Spearman rank-order correlation coefficient is  $-0.29$ , indicating a weak correlation between the diffusional kurtosis and the diffusion coefficient. This suggests that  $K_{app}$  provides additional information on the water diffusion properties in the brain. The data points in Fig. 4 with diffusion coefficients above  $1.5 \mu\text{m}^2/\text{ms}$  probably correspond to voxels containing some cerebrospinal fluid.

Table 1 gives mean MRI estimates for the diffusional kurtosis and the diffusion coefficient in cortical gray matter and frontal white matter based on our data from six subjects. The overall average diffusional kurtosis is  $0.82 \pm 0.03$  in gray matter and  $1.41 \pm 0.11$  in white matter, which is consistent with the greater degree of tissue structure in white matter (here the uncertainties indicate standard errors). The anisotropy of the diffusional kurtosis in white matter is not clearly evident in the data of Table 1 due to the averaging of data from several subjects.

### Phantom Study

Figure 5 shows parametric maps for apparent diffusion coefficient and diffusional kurtosis obtained for the phantom in the slice direction. The signal intensity in the surrounding water bath has been nulled for the sake of clarity. The five sucrose bottles (a–e) have diffusion coefficients similar to those measured by Laubach and co-workers (14). Their mean diffusional kurtosis values are all below 0.1, consistent with nearly Gaussian diffusion. The asparagus bottle (f) has a diffusion coefficient intermediate to that of bottles a and b, but the diffusional kurtosis is  $0.39 \pm 0.06$ , reflecting a significant departure from Gaussian diffusion.

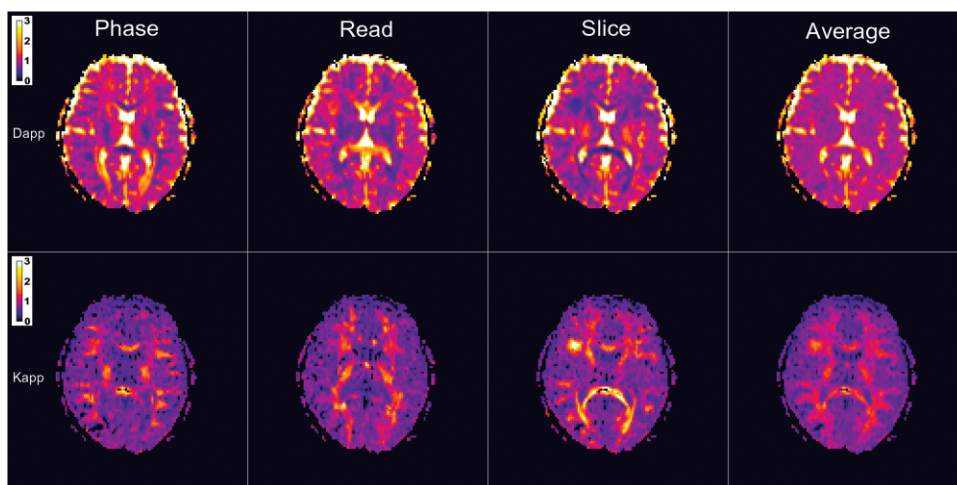
Table 2 gives the mean diffusion coefficient and diffusional kurtosis for bottles b (10% sucrose) and the asparagus bottle in the phase, read, and slice directions. The two bottles have a similar diffusion coefficient, but the diffusional kurtosis is much higher in the asparagus bottle. Both the diffusion coefficient and the diffusional kurtosis varied little with direction, suggesting that the phantoms were essentially isotropic.

### DISCUSSION

In the conventional analysis of DWI data, the logarithm of the signal intensity is fit to a linear function of  $b$  and an estimate for the diffusion coefficient is extracted. The DKI approach presented here differs essentially in that the imaging data are fit to a quadratic function, which allows for estimates of both the diffusion coefficient and the diffusional kurtosis. In order to obtain the diffusional kurtosis with a reasonable degree of precision,  $b$  values somewhat larger than those usually employed in DWI are necessary so that the departure from linearity is clearly apparent. In the brain, maximum  $b$  values of about  $2000 \text{ s/mm}^2$  are sufficient.

An alternative method for obtaining the diffusional kurtosis is to use  $q$ -space imaging techniques to extract the full diffusion displacement probability distribution (4,5). However, this will typically require  $b$  values larger than

FIG. 3. Parametric maps of the apparent diffusion coefficient (first row) and the apparent diffusional kurtosis (second row) for one subject. The scale bar for the diffusion coefficient is in units  $\mu\text{m}^2/\text{ms}$ . The average kurtosis map shows markedly better gray matter/white matter contrast than the average diffusion map.



needed for our DKI approach. Perhaps more importantly, we have shown that the diffusional kurtosis is the essential information contained in the initial departure of the logarithm of the signal intensity from linearity in  $b$ . After the diffusion coefficient, the diffusional kurtosis is therefore the diffusion property that is the most readily accessible with MRI.

Our data show that the apparent diffusional kurtosis in frontal white matter is about 70% higher than in cortical gray matter, reflecting white matter's higher degree of structure. Our gray matter average value of  $0.82 \pm 0.03$  is similar to the average gray matter values of  $0.66 \pm 0.28$  and  $0.78 \pm 0.12$  reported by Jensen and Helpert (2), which were derived from a retrospective analysis of two different experiments. However, using  $q$ -space methods, a larger value of  $2.68 \pm 0.09$  has been obtained by Lätt et al. (4) based on the study of five subjects, and a smaller value of  $0.30 \pm 0.05$  has been obtained by Chabert et al. (5) based on the study of seven subjects. In white matter, our average value of  $1.41 \pm 0.11$  is comparable to the values of  $1.03 \pm 0.27$  and  $1.42 \pm 0.11$  of Jensen and Helpert (2). In contrast, Lätt et al. (4) report a white matter value of  $3.16 \pm 0.17$ , while Chabert et al. (5) report white matter values ranging from 0.26 to 1.16. These discrepancies in the measured diffusional kurtosis may, in part, be due to differences in experimental technique (e.g., diffusion time interval), analysis method, region of interest selection, and subject variability.

Our phantom results support the ability of diffusional kurtosis maps to detect structural properties that are not evident in diffusion coefficient maps. Our phantom, which was essentially isotropic, demonstrates that a nonzero diffusional kurtosis does not require diffusional anisotropy. We hypothesize that the diffusional kurtosis observed in the pureed asparagus is due to irregularly oriented diffusion barriers. The nonzero diffusional kurtosis observed in gray matter may have a similar origin.

A limitation of DKI is that the rigorous correspondence, given by Eq. [6], between the true diffusional kurtosis and the apparent diffusional kurtosis holds only in the limit of infinitesimal gradient pulse durations. The same limitation applies also to conventional DWI (1). However, if the tissue can be modeled as consisting of multiple compart-

ments, inside of which the diffusion is Gaussian, then  $K_{\text{app}} = K$  independent of the value of the gradient pulse duration. The diffusional kurtosis can still be nonzero, as indicated by Eq. [7], if the various compartments have different diffusion coefficients. This suggests that the apparent diffusional kurtosis, which for practical reasons is normally obtained with relatively long gradient pulses, may still be a fair approximation to the true diffusional kurtosis. Moreover, for Gaussian diffusion  $K_{\text{app}} = 0$  regardless of the gradient pulse duration, and so a nonzero  $K_{\text{app}}$  is a general indicator of non-Gaussian diffusion. Nevertheless, further investigation of the significance of this limitation is warranted.

A principal advantage of the diffusional kurtosis compared with the diffusion coefficient is that it is a specific

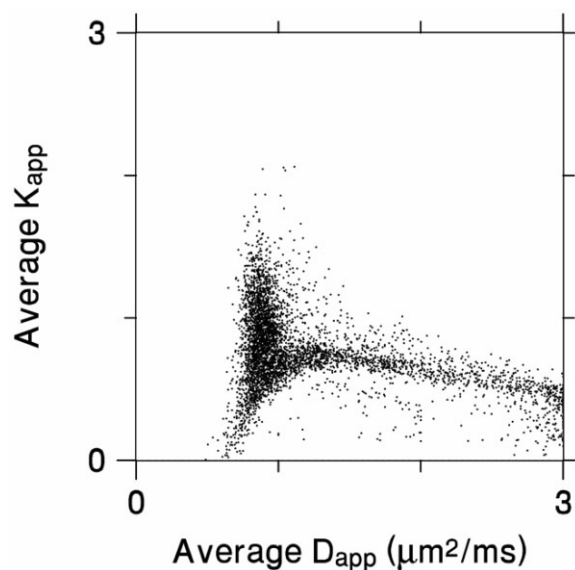


FIG. 4. Scatter plot showing the correlation between the average apparent diffusion coefficient and the average apparent diffusional kurtosis for the maps of Fig. 3. The Spearman rank-order correlation coefficient is  $-0.29$ , indicating that the two quantities are only weakly correlated. This implies that the diffusional kurtosis gives information beyond that provided by the diffusion coefficient.

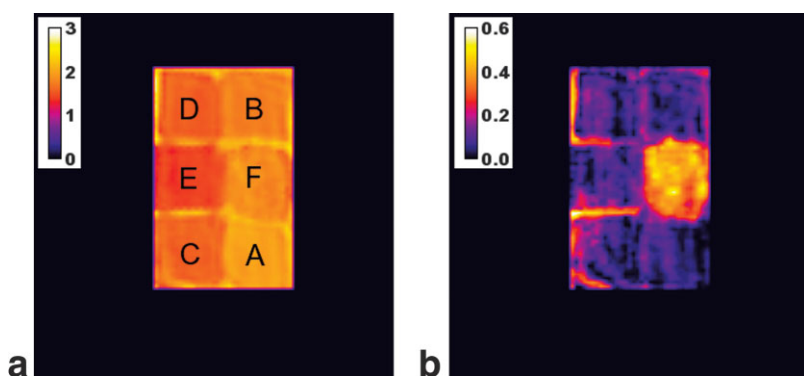


FIG. 5. Parametric maps of the apparent diffusion coefficient (left) and the apparent diffusional kurtosis (right) for the phantom in the slice direction. The scale bar for the diffusion coefficient is in units of  $\mu\text{m}^2/\text{ms}$ . Bottles a through e contain sucrose solutions with sucrose concentrations ranging from 5 to 25%. Bottle f contains pureed asparagus. The average kurtosis map clearly reveals the higher degree of structure in asparagus bottle, which is not evident in the diffusion coefficient map.

measure of tissue structure (e.g., cellular compartments and membranes). Although the diffusion coefficient is affected by tissue structure, it is also influenced by other factors, such as the concentration of macromolecules, and is hence a less specific indicator of a tissue's structural complexity, as is apparent from our phantom results. This may also be illustrated by comparing the average  $D_{\text{app}}$  and  $K_{\text{app}}$  maps of Fig. 3. In the average  $D_{\text{app}}$  map, there is little contrast between white and gray matter, while a sharp difference between white and gray matter is apparent in the average  $K_{\text{app}}$  map. Similarly, the scatter plot of Fig. 4 shows that  $K_{\text{app}}$  can vary considerably for regions with similar diffusion coefficients.

The information given by the diffusional kurtosis is also substantially different from that given by the fractional anisotropy and related indices that are obtained with DTI (8,12). In particular, the sensitivities of DKI and DTI differ dramatically in largely isotropic tissues such as gray matter. This is because the fractional anisotropy reflects structure only if it is spatially oriented. Hence, alterations in the structure of gray matter that may occur as a consequence of pathology would not change the fractional anisotropy, but could shift the diffusional kurtosis.

The primary purpose of this article is to establish the theory and feasibility of DKI. Further work is needed to evaluate its importance for clinical studies. However, some preliminary speculations can be made on possible applications of DKI. First, the large values of the diffusional kurtosis in white matter suggest that DKI may be

useful for studying white matter diseases, such as multiple sclerosis and epilepsy. Second, a retrospective analysis of animal data indicates that the diffusional kurtosis in the brain increases by nearly threefold following ischemia (2), which implies that DKI is sensitive to structural changes that occur in tissue following stroke. Interestingly, this apparent increase in the degree structure following ischemia could be consistent with a decrease in membrane permeability (15). Third, the diffusional kurtosis has been shown to be small in newborns (2). The increase in the diffusional kurtosis that presumably occurs through childhood could then be used to quantify tissue structure changes in the developing brain. Finally, DKI may also be applied to lung imaging with hyperpolarized  $^3\text{He}$ , since a nonmonoexponential dependence of the NMR signal on  $b$  has been clearly observed in this case (16).

A natural generalization of DKI is diffusional kurtosis tensor imaging (DKTI), in which the full diffusional kurtosis tensor is determined. Since this tensor has 15 independent components, DKTI requires the use of at least 15 different directions for the diffusion sensitizing gradients. From the diffusional kurtosis tensor, additional physical quantities such as the angle-averaged diffusional kurtosis and the diffusional kurtosis anisotropy can be deduced. A detailed discussion of DKTI will be the subject of a future publication.

## CONCLUSION

DKI is a straightforward extension of DWI that provides a sensitive measure of tissue structure by quantifying the degree to which water diffusion is non-Gaussian. In the brain, maximum  $b$  values of about  $2000 \text{ s/mm}^2$  are needed, which are about twice those usually used for DWI and are now readily attainable on modern clinical MRI scanners. The image postprocessing required to generate diffusional kurtosis maps is only slightly more complex than that needed to obtain diffusion coefficient maps. Thus, DKI represents a modest change in the standard diffusion imaging methodology, while providing a significantly more complete characterization of water diffusion and tissue structure.

## APPENDIX

Here we outline the derivations of some of the basic results presented under Theory.

Table 2

MRI Estimates for the Mean Diffusional Kurtosis and Diffusion Coefficient Obtained from Bottles b (10% Sucrose Solution) and f (Asparagus) of the Phantom

Bottle	Direction	Diffusional kurtosis	Diffusion coefficient ( $\mu\text{m}^2/\text{ms}$ )
B	Phase	$0.02 \pm 0.02$	$1.66 \pm 0.02$
B	Read	$0.04 \pm 0.03$	$1.66 \pm 0.03$
B	Slice	$0.06 \pm 0.03$	$1.72 \pm 0.03$
F	Phase	$0.32 \pm 0.07$	$1.72 \pm 0.05$
F	Read	$0.34 \pm 0.09$	$1.75 \pm 0.12$
F	Slice	$0.39 \pm 0.06$	$1.81 \pm 0.07$

Note. Both bottles have a similar diffusion coefficient, but the diffusional kurtosis in the asparagus bottle is much larger than that of the sucrose bottle, reflecting the greater degree of structure. The uncertainties indicate standard deviations.

Consider the NMR signal produced in a region of interest following an initial  $90^\circ$  spin flip pulse. Following the formalism of Jensen and Chandra (17), the signal intensity at a time  $T$  can be written

$$S(\mathbf{f}) = S(0) \left\langle \exp \left[ -i\gamma \int_0^T dt \sigma(t) \mathbf{f}(t) \cdot \mathbf{r}(t) \right] \right\rangle, \quad [\text{A1}]$$

where the function  $\mathbf{f}(t)$  specifies diffusion sensitizing gradients and  $\sigma(t)$  specifies the spin flip function. The angle brackets indicate an average over all the diffusion paths  $\mathbf{r}(t)$  within the region of interest. This is a generalization of the averaging defined by Eq. [1], and hence the same notation is used. The spin flip function  $\sigma(t)$  has a magnitude of unity and changes sign at the times of any  $180^\circ$  refocusing pulses, as discussed in detail by Jensen and Chandra (17). The validity of Eq. [A1] requires that any variations in the  $T_2$  relaxation rate within the region of interest due to mechanisms other than the applied diffusion sensitizing gradients be negligible.

From Eq. [A1], the expansion of the logarithm of  $S$  in powers of  $\mathbf{f}$  is seen to be

$$\ln [S(\mathbf{f})] = \ln [S(0)] - \gamma^2 B_1 + \gamma^4 B_2 + O(f_i^6), \quad [\text{A2}]$$

where

$$B_1 = \frac{1}{2} \sum_{i=1}^3 \sum_{j=1}^3 \int_0^T dt \int_0^T dt' \sigma(t) \sigma(t') f_i(t) f_j(t') \langle r_i(t) r_j(t') \rangle \quad [\text{A3}]$$

$$B_2 = \frac{1}{24} \sum_{i=1}^3 \sum_{j=1}^3 \sum_{k=1}^3 \sum_{l=1}^3 \int_0^T dt \int_0^T dt' \int_0^T dt'' \int_0^T dt''' \sigma(t) \sigma(t') \sigma(t'') \sigma(t''') \times \sigma(t''') f_i(t) f_j(t') f_k(t'') f_l(t''') \times [\langle r_i(t) r_j(t') r_k(t'') r_l(t''') \rangle - 3 \langle r_i(t) r_j(t') \rangle \langle r_k(t'') r_l(t''') \rangle] \quad [\text{A4}]$$

with  $f_i$  and  $r_i$  being the components of the vectors  $\mathbf{f}$  and  $\mathbf{r}$ , respectively. In deriving Eq. [A2], we have used the condition of no net flow  $\langle \mathbf{r}(t) \rangle = \langle \mathbf{r}(0) \rangle$  and the general refocusing requirement (17)

$$\int_0^T dt \sigma(t) \mathbf{f}(t) = 0. \quad [\text{A5}]$$

Now assume that

$$\sigma(t) \mathbf{f}(t) = c [\delta(t - t_b) - \delta(t - t_a)] \mathbf{n}, \quad [\text{A6}]$$

where  $\mathbf{n}$  is the direction of the diffusion sensitizing gradients,  $c$  sets the gradient strength, and  $\delta(t)$  is the Dirac delta function. This is equivalent to assuming arbitrarily short gradient pulse durations. Substituting Eq. [A6] into Eqs. [A3] and [A4] yields

$$B_1 = \frac{1}{2} c^2 \langle (\mathbf{n} \cdot \mathbf{s})^2 \rangle \quad [\text{A7}]$$

$$B_2 = \frac{1}{24} c^4 [\langle (\mathbf{n} \cdot \mathbf{s})^4 \rangle - 3 \langle (\mathbf{n} \cdot \mathbf{s})^2 \rangle^2], \quad [\text{A8}]$$

where  $\mathbf{s} = \mathbf{r}(t_b) - \mathbf{r}(t_a)$ .

From Eqs. [2], [A7], and [A8], we find

$$B_2 = \frac{1}{6} B_1^2 K. \quad [\text{A9}]$$

By identifying  $\gamma^2 B_1$  with  $bD_{\text{app}}$ , Eqs. [5], [A2], and [A9] are seen to imply the result of Eq. [6]. Note that the validity of Eq. [6] does not depend on how many  $180^\circ$  refocusing pulses are used.

The result of Eq. [7] may be derived for isotropic diffusion by assuming that the diffusion displacement probability distribution is

$$P(\mathbf{s}, t) = \sum_{i=1}^N p_i (4\pi D_i t)^{-3/2} \exp(-\mathbf{s} \cdot \mathbf{s} / 4D_i t) \quad [\text{A10}]$$

and applying Eqs. [1] and [2]. It is also straightforward to demonstrate that Eq. [7] holds for anisotropic diffusion provided that  $K$ ,  $\bar{D}$ , and  $\text{var}(D)$  are interpreted as the diffusional kurtosis, average diffusion coefficient, and diffusion variance for a particular direction.

The result of Eq. [9] can be obtained by expanding in powers of  $b$  the analytic expression for  $S(b)$  for the two-compartment exchange model (1,11) and then utilizing Eqs. [5] and [6]. The relationship  $\tau_a p_b = \tau_b p_a$  (indicated under Theory) is the condition for equilibrium.

To obtain the result of Eq. [10], we first consider the diffusion displacement probability distribution for a single spherical pore of radius  $R$ . In this case, one may show that the long time limit is given by

$$\lim_{t \rightarrow \infty} P(\mathbf{s}, t) = \left( \frac{3}{4\pi R^3} \right)^2 \int d^3 r \theta(R - |\mathbf{s} + \mathbf{r}|) \theta(R - |\mathbf{r}|) = \frac{1}{64\pi} \theta(2R - |\mathbf{s}|) \left( 48 - 36 \frac{|\mathbf{s}|}{R} + 3 \frac{|\mathbf{s}|^3}{R^3} \right) \equiv g(\mathbf{s}, R) \quad [\text{A11}]$$

with  $\theta(x)$  being the Heaviside step function. Equation [10] is then derived from Eqs. [1] and [2] with the diffusion displacement probability distribution

$$P(\mathbf{s}, t) = p_a g(\mathbf{s}, R_a) + p_b g(\mathbf{s}, R_b), \quad [\text{A12}]$$

which is appropriate for the long time limit of a region of interest having a water fraction  $p_a$  in pores of radii  $R_a$  and a water fraction  $p_b$  in pores of radii  $R_b$ .

## ACKNOWLEDGMENTS

We thank Annette Nusbaum and Matilde Inglese for assistance with the selection of the regions of interest for the brain images.

## REFERENCES

1. Kärger J. NMR self-diffusion studies in heterogeneous systems. *Adv Colloid Interface Sci* 1985;23:129–148.
2. Jensen JH, Helpert JA. Quantifying non-Gaussian water diffusion by means of pulsed-field-gradient MRI. In: *Proceedings of the 11th Annual Meeting of ISMRM, Toronto, Canada, 2003*. p 2154.
3. Cohen Y, Assaf Y. High b-value q-space analyzed diffusion-weighted MRS and MRI in neuronal tissues—a technical review. *NMR Biomed* 2002;15:516–542.
4. Lätt J, Brockstedt S, Wirestam R, Larsson E, Ståhlberg F. Visualization of displacement-distribution parameters in q-space imaging. In: *Proceedings of the 11th Annual Meeting of ISMRM, Toronto, Canada, 2003*. p 590.
5. Chabert S, Meca CC, Le Bihan D. Relevance of the information about the diffusion distribution in vivo given by kurtosis in q-space imaging. In: *Proceedings of the 12th Annual Meeting of ISMRM Kyoto, Japan, 2004*. p 1238.
6. Balanda KP, MacGillivray HL. Kurtosis: a critical review. *Am Stat* 1988;42:111–119.
7. Press WH, Teukolsky SA, Vetterling WT, Flannery BP. *Numerical recipes in C: the art of scientific computing*. New York: Cambridge University Press; 1992.
8. Bammer R. Basic principles of diffusion-weighted imaging. *Eur J Radiol* 2003;45:169–184.
9. Yablonskiy DA, Bretthorst GL, Ackerman JJ. Statistical model for diffusion attenuated MR signal. *Magn Reson Med* 2003;50:664–669.
10. Liu C, Bammer R, Acar B, Moseley ME. Characterizing non-Gaussian diffusion by using generalized diffusion tensors. *Magn Reson Med* 2004;51:924–937.
11. Lee JH, Springer CS Jr. Effects of equilibrium exchange on diffusion-weighted NMR signals: the diffusigraphic “shutter-speed”. *Magn Reson Med* 2003;49:450–458.
12. Dong Q, Welsh RC, Chenevert TL, Carlos RC, Maly-Sundgren P, Gomez-Hassan DM, Mukherji SK. Clinical applications of diffusion tensor imaging. *J Magn Reson Imaging* 2004;19:6–18.
13. Reese TG, Heid O, Weisskoff RM, Wedeen VJ. Reduction of eddy-current-induced distortion in diffusion MRI using a twice-refocused spin echo. *Magn Reson Med* 2003;49:177–182.
14. Laubach HJ, Jakob PM, Loevblad KO, Baird AE, Bovo MP, Edelman RR, Warach S. A phantom for diffusion-weighted imaging of acute stroke. *J Magn Reson Imaging* 1998;8:1349–1354.
15. Helpert JA, Ordidge RJ and Knight RA. The effect of cell membrane water permeability on the apparent diffusion coefficient of water. In: *Proceedings of the 11th Annual Meetings of Society of Magnetic Resonance in Medicine Berlin, Germany, 1992*. p 1201.
16. Yablonskiy DA, Sukstanskii AL, Leawoods JC, Gierada DS, Bretthorst GL, Lefrak SS, Cooper JD, Conradi MS. Quantitative in vivo assessment of lung microstructure at the alveolar level with hyperpolarized  $^3\text{He}$  diffusion MRI. *Proc Natl Acad Sci USA* 2002;99:3111–3116.
17. Jensen JH, Chandra R. Weak-diffusion theory of NMR signal decay in magnetically heterogeneous media. *J Magn Reson* 1997;126:193–199.